



Forbes, Duncan A.; Carl J. Grillmair; Williger, Elson; Jean P. Brodie. (1998). HST imaging of the globular clusters in the Fornax cluster: NGC 1399 and NGC 1404. *Monthly notices of the Royal Astronomical Society*. 293, (3): 325-336.

Available at: <http://dx.doi.org/10.1046/j.1365-8711.1998.01202.x>

© 1998 The Royal Astronomical Society.

This is the author's version of the work. It is posted here with the permission of the publisher for your personal use. No further distribution is permitted. If your library has a subscription to this journal, you may also be able to access the published version via the library catalogue.

The definitive version is available at [www.interscience.wiley.com](http://www.interscience.wiley.com)

# HST Imaging of the Globular Clusters in the Fornax Cluster: NGC 1399 and NGC 1404

Duncan A. Forbes<sup>1</sup>, Carl J. Grillmair<sup>2</sup>, Gerard M. Williger<sup>3</sup>, R. A. W. Elson<sup>4</sup>  
and Jean P. Brodie<sup>5</sup>

<sup>1</sup>*School of Physics and Astronomy, University of Birmingham, Edgbaston, Birmingham B15 2TT*

(E-mail: forbes@star.sr.bham.ac.uk)

<sup>2</sup>*Jet Propulsion Laboratory, 4800 Oak Grove Drive, Pasadena, CA 91109, USA*

(E-mail: carl@grandpa.jpl.nasa.gov)

<sup>3</sup>*MPIA, Königstuhl 17, D-69117 Heidelberg, Germany and NOAO, Code 681, Goddard Space Flight Center, Greenbelt, MD 20771, USA*

(E-mail: williger@tejut.gsfc.nasa.gov)

<sup>4</sup>*Institute of Astronomy, Madingley Road, Cambridge CB3 0HA*

(E-mail: elson@star.ast.cam.ac.uk)

<sup>5</sup>*Lick Observatory, University of California, Santa Cruz, CA 95064, USA*

(E-mail: brodie@ucolick.org)

5 February 2008

## ABSTRACT

The Fornax cluster galaxies NGC 1399 and NGC 1404 are ideal for studying the effects of a cluster environment on globular cluster systems. Here we present new optical imaging of these two galaxies from both the *Hubble Space Telescope's* Wide Field and Planetary Camera 2 and the Cerro Tololo Inter-American Observatory's 1.5m telescope. The combination of both data sets provides unique insight on the spatial and colour distribution of globular clusters. From B–I colours, we find that both galaxies have a broad globular cluster metallicity distribution that is inconsistent with a single population. Two Gaussians provide a reasonable representation of the metallicity distribution in each galaxy. The metal-rich subpopulation is more centrally concentrated than the metal-poor one. We show that the radial metallicity gradient can be explained by the changing relative mix of the two globular cluster subpopulations. We derive globular cluster surface density profiles, and find that they are flatter (i.e. more extended) than the underlying starlight. The total number of globular clusters and specific frequency are calculated to be  $N = 5700 \pm 500$ ,  $S_N = 11.5 \pm 1.0$  for NGC 1399 and  $N = 725 \pm 145$ ,  $S_N = 2.0 \pm 0.5$  for NGC 1404. Our results are compared to the expectations of globular cluster formation scenarios.

**Key words:** galaxies: individual: NGC 1399, NGC 1404 - galaxies: interactions - galaxies: elliptical - globular clusters: general

## 1 INTRODUCTION

Globular cluster (GC) systems are in some respects (e.g. luminosity function), more similar to one another than are their host galaxies. This suggests an underlying uniformity in the physical conditions under which GC systems and galaxies formed. On the other hand, properties such as the total number of clusters per unit galaxy luminosity show significant variations, and fundamental questions concerning the origins of these variations remain unanswered. In particular, the roles of tidal encounters, mergers, cooling flows, and initial conditions in the formation of GC systems have yet to be understood.

Two galaxies of particular interest in this regard are

NGC 1399 at the center of the Fornax cluster and a nearby cluster member NGC 1404. By studying the GC systems of these two galaxies we hope to better understand the environmental influences on the formation of GCs and their host galaxies. Various estimates of the distance modulus to the Fornax cluster have been made in recent years. Here we adopt a typical value of  $m-M = 31.2$ , which places the cluster 0.2 mag more distant than Virgo (Jacoby *et al.* 1992). With this distance modulus and no Galactic extinction correction, the optical luminosity of NGC 1399 is  $M_V = -21.74$  (Faber *et al.* 1989). This cD galaxy is surrounded by hot X-ray emitting gas which extends out to at least  $38'$  or 190 kpc (Mason & Rosen 1985; Ikebe *et al.* 1996). The mass-to-light ratio increases with galactocentric distance reaching a value

of  $M/L \sim 70 M_{\odot}/L_{\odot}$  at  $\sim 5'$  (Grillmair *et al.* 1994a). Well within the X-ray envelope, even allowing for projection effects, at about  $10'$  (50 kpc) to the south-east of NGC 1399 lies NGC 1404. It is classified as an E1 galaxy and has an optical luminosity of  $M_V = -21.37$  (Faber *et al.* 1989).

The GC systems of NGC 1399 and NGC 1404 have been studied using ground-based imaging by a number of workers (NGC 1399: Hanes & Harris 1986; Giesler & Forte 1990; Wagner *et al.* 1991; Bridges *et al.* 1991; Ostrov *et al.* 1993; Kissler-Patig *et al.* 1997a and NGC 1404: Hanes & Harris 1986; Richtler *et al.* 1992). For NGC 1399, Kissler-Patig *et al.* (1997a) gives the total number of GCs to be  $N_{GC} = 5940 \pm 570$ . This gives a high specific frequency  $S_N = 11 \pm 4$ . A kinematic study of the GCs around NGC 1399 showed that the outer GCs appear to be dynamically related more to the cluster of galaxies than they are to NGC 1399 itself (Grillmair *et al.* 1994a). This suggests that accretion of intracluster GCs (West *et al.* 1995), tidal stripping (Forte *et al.* 1982; Forbes, Brodie & Grillmair 1997) or mergers (Ashman & Zepf 1992) may help to explain the high specific frequency of NGC 1399. For NGC 1404 the number of GCs is less certain. Hanes & Harris (1986) from a photographic study estimated  $N_{GC} = 190 \pm 80$ , while more recently Richtler *et al.* (1992) found  $N_{GC} = 880 \pm 120$ . The resulting  $S_N$  values range from  $0.5 \pm 0.3$  to  $2.5 \pm 0.3$  respectively. The latter value is close to the average for ellipticals in the Fornax cluster.

Here we present imaging data from *HST*'s Wide Field and Planetary Camera 2 (WFPC2) and the Cerro Tololo Inter-American Observatory's (CTIO) 1.5m telescope of NGC 1399 and NGC 1404. The WFPC2 data provide accurate magnitudes and colours with virtually no contamination from foreground stars or background galaxies. These data are complemented by wide field-of-view CCD imaging from CTIO. In this paper we will focus on the colour (metallicity) and spatial distribution of GCs. The GC luminosity functions in these two galaxies and others in the Fornax cluster are addressed by Grillmair *et al.* (1997), and a detailed study of NGC 1379, using WFPC2 and CTIO data, is given by Elson *et al.* (1997).

## 2 OBSERVATIONS AND DATA REDUCTION

### 2.1 HST Imaging

Details of our HST imaging program are given by Grillmair *et al.* (1997). Here we use four pointings from that programme, namely a central pointing on each of NGC 1399 and NGC 1404, an outer pointing for NGC 1399 and a background field. The outer pointing (F0338) is situated in the cD envelope of NGC 1399, on the opposite side of the galaxy from NGC 1404. The background field (F0336) is situated approximately 1.4 degrees south of NGC 1399 in a blank region of sky and serves to measure the surface density of background sources.

Exposure times totaled 1800s in F814W and 5200s in F450W for NGC 1399; 1860s and 5000s for NGC 1404 using the WFPC2 camera. Three images were taken at one pointing, the other two were offset by  $0.5''$  which corresponds roughly to integer pixel shifts in both the PC and WFC chips. The images were then aligned and median-combined

using VISTA software which effectively removed both cosmic rays and hot pixels. The resulting images were found to be statistically superior to those reduced using standard STSDAS tasks, and enabled us to push our completeness limit to about  $B = 26.5$  without incurring large numbers of spurious detections.

Compact sources in each pointing have been detected and measured using DAOPHOT II/ALLSTAR software as described in Grillmair *et al.* (1997). For the PC chips the galaxy was subtracted off first. Magnitudes have been converted into standard Johnson-Cousins B and I. No Galactic extinction correction has been applied. A colour-magnitude diagram for all of the detected sources in each of the four pointings is shown in Fig. 1. Completeness tests indicate that the 50% incompleteness occurs at  $B \sim 26.5$  for all four pointings, with small variations between each pointing. (Note for the PC chips it is about 0.5 mag brighter.) In order to avoid any colour bias in our results we have excluded all sources fainter than this limit. We have also excluded sources brighter than  $B = 21$  as these objects would be more luminous than Galactic GCs, and so are probably foreground stars. We also applied a colour cut to the data, so that only sources with  $1.2 < B-I < 2.5$  are included. This cut is roughly equivalent to  $-2.5 < [Fe/H] < +1.0$ , assuming the Galactic colour-metallicity relation of Couture *et al.* (1990), and covers the range of expected GC metallicities. For NGC 1399, 95% of all sources lie within this colour selection and for NGC 1404 it is 90%. This magnitude and colour selection are indicated in Fig. 1 by dashed lines. With these selection cuts applied our final sample consists of 572 objects in NGC 1399 central, 59 in NGC 1399 outer and 208 in NGC 1404. The background field has only 14 objects. This background field allows us to fairly accurately estimate the proportion of *bona fide* GCs in the three galaxy pointings, i.e.  $\geq 98\%$  in NGC 1399 central,  $\geq 76\%$  in NGC 1399 off-center and  $\geq 93\%$  in NGC 1404.

### 2.2 Ground-based Imaging

Broad-band B and I images of NGC 1399 and NGC 1404 were taken with the CTIO 1.5m telescope. We used a Tek 2048 x 2048 array with a pixel scale of  $0.44''/\text{pixel}$ , yielding a field-of-view  $15'$  on a side. The galaxies were observed in 1995 December with typical seeing conditions of  $\sim 1.5''$ . Data reduction was carried out in the standard way (i.e. bias and dark subtraction, flat-fielding and sky subtraction). The total exposure times were 9600s in B and 3660s in I for NGC 1399; 9100s in B and 3060s in I for NGC 1404. After combining, the images were calibrated using aperture photometry from the catalogs of Longo & de Vaucouleurs (1983) and de Vaucouleurs & Longo (1988). This procedure gave an rms accuracy of  $\pm 0.08$  mag for NGC 1399 and  $\pm 0.05$  mag for NGC 1404. No Galactic extinction correction was applied.

Globular clusters were detected automatically using DAOPHOT. The detection threshold was set at a conservative  $5\sigma$  per pixel i.e., five times the background noise. Selection cuts in the DAOPHOT 'sharpness' and 'roundness' parameters were made to help remove cosmic rays and extended objects from the candidate lists. (These parameters help to remove spikey objects and very non-round ob-

jects.) For each detected object we measured a 3 pixel radius aperture magnitude and applied an aperture correction based on a curve-of-growth type analysis for a dozen isolated GCs. The rms from the aperture correction is  $\sim 0.05$  mag. Colour–magnitude diagrams for all of the detected sources for the two galaxies are shown in Fig. 2. For the CTIO data we decided to adopt the same colour selection criteria as the HST data, and the same bright magnitude cutoff. For the faint magnitude cutoff, we use the 50% incompleteness value. Based on an examination of the luminosity function, we estimate that for NGC 1399 the 50% value is  $B \sim 24.3$  and for NGC 1404 it is  $B \sim 24.2$ . Thus our CTIO selection criteria are  $1.2 < B-I < 2.5$  and  $21 < B < 24.2/24.3$ , as is indicated in Fig. 2 by dashed lines. Even with our selection criteria we expect some contamination from foreground stars and background galaxies in our samples of 1752 objects in NGC 1399 and 858 objects in NGC 1404. This issue will be discussed below. We note that although the CTIO data only sample the brighter GCs, we do not expect this to bias the metallicity distribution. For GCs in the Milky Way and M31 (Huchra, Brodie & Kent 1991) and in NGC 5846 (Forbes, Brodie & Huchra 1996) there appears to be no luminosity–metallicity dependence.

### 3 RESULTS AND DISCUSSION

#### 3.1 Spatial Distribution

Given the magnitude depth and the availability of a background field, our HST data are ideal to examine the surface density distribution of GCs. We first calculate the GC density in 5 annuli around NGC 1399. We make use of the fact that out to  $100''$  radius the WFPC2 gives almost complete  $180^\circ$  coverage for one hemisphere of the galaxy (see Forbes, Franx & Illingworth 1995 for details). For the NGC 1399 outer and background fields we simply add up the total number of GCs, i.e. 59 and 14 respectively. We have also made a small correction ( $\sim 15\%$ ) for the expected number of undetected GCs at the faint end of the luminosity function as determined by Grillmair *et al.* (1997). Next, we divide the number of GCs by the appropriate spatial coverage to give a surface density. Finally, we subtract off the background density of 2.9 objects per square arcmin giving the background–corrected surface density of GCs. This is shown in Fig. 3.

Excluding the innermost 2 data points for NGC 1399 we have fit the data with a function of the form:

$$\rho = \rho_0 r^\alpha$$

This fit is shown by a solid line for which  $\rho_0 = 126 \text{ arcmin}^{-2}$  and  $\alpha = -1.2 \pm 0.2$ . It is clear from the NGC 1399 outer pointing that there are GCs at a projected radius of 8.2 arcmin from NGC 1399. Extrapolating the profile to 9.7 arcmin (the projected distance of NGC 1404) suggests that there is about one GC per square arcmin associated with NGC 1399. This corresponds to half a dozen GCs in the WFPC2 field-of-view centered on NGC 1404. The procedure for estimating the surface density profile of NGC 1404 is similar to that of NGC 1399, except that we subtract both the background density and the expected density of GCs in each annulus due to NGC 1399. Again the HST data is fit using a powerlaw profile (excluding the innermost data point) with  $\rho_0 = 36 \text{ arcmin}^{-2}$  and  $\alpha = -1.3 \pm 0.2$ .

For both galaxies the GC surface density rises towards the galaxy center but flattens off (in log space) in the very inner regions giving a definable ‘core’ to the GC system where the profile changes slope. This does not appear to be a selection effect and has been observed in other large galaxies (e.g. Grillmair *et al.* 1986, 1994b). Forbes *et al.* (1996) found that the ‘core radius’ of the GC system is loosely correlated with the galaxy luminosity. We estimate that the GC systems of NGC 1399 and NGC 1404 have core radii of  $40''$  (3.4 kpc) and  $30''$  (2.5 kpc) respectively. These values are within the scatter of the relation found by Forbes *et al.* (1996) and are similar to the galaxy effective radii. We have measured a GC surface density slope of  $-1.2 \pm 0.2$  for NGC 1399. There have been three previous CCD studies which measured the GC slope. Wagner *et al.* (1991) found that interior to  $\sim 120''$  the GC slope was  $-1.4 \pm 0.11$ , and this steepened to  $-1.54 \pm 0.15$  for larger radii. Kissler–Patig *et al.* (1997a) derived  $-1.55 \pm 0.25$  and  $-1.75 \pm 0.3$  from two pointings for radii beyond  $\sim 50''$ . Bridges *et al.* (1991) measured  $-1.4 \pm 0.2$  from their B band data and  $-1.5 \pm 0.2$  from their V band data. Our value is somewhat flatter than those measured by others. One possible reason for this is that our outer pointing is located in the cD envelope of NGC 1399 where the GC surface density ‘flattens out’ (e.g. Kissler–Patig *et al.* 1997a). If we exclude the outer point, our fitted slope steepens to  $-1.25$ . Another possibility is that, even though we have not included the inner two data points in the fit, we are still fitting into the core–flattened region. The stellar profile (log intensity) for NGC 1399 is also shown in Fig. 3. We measure a slope of  $-1.6 \pm 0.1$  for the galaxy light. This compares with the measurements of  $-1.67 \pm 0.12$  (Wagner *et al.* 1991) and  $-1.75 \pm 0.1$  (Kissler–Patig *et al.* 1997a). There are been some debate as to whether the GC profile is flatter than the galaxy profile in NGC 1399. In particular, Bridges *et al.* (1991) claimed that the GC system had the same slope as the galaxy. Whereas both Wagner *et al.* (1991) and Kissler–Patig *et al.* (1997a) said it was somewhat flatter. Excluding our data, the weighted mean value from previous studies is  $-1.47 \pm 0.09$  for the GC slope and  $-1.72 \pm 0.06$  for the galaxy slope. This indicates that the GC profile is  $0.25 \pm 0.11$  flatter than the galaxy starlight. Our data suggest that the difference is even greater, i.e.  $0.4 \pm 0.22$ . Thus, we conclude that the GC surface density profile is flatter than the galaxy starlight by about 0.3 in the log at about the  $2 \sigma$  significance level. For NGC 1404, we measure a GC slope of  $-1.3 \pm 0.2$  and a galaxy starlight slope of  $-1.9 \pm 0.1$ . Thus the GC systems in both galaxies have a flatter, more extended distribution than the underlying starlight.

Using the surface density profile we can estimate the total number of GCs and the specific frequency ( $S_N$ ; Harris & van den Bergh 1981) for NGC 1399 and NGC 1404. For NGC 1399 GCs are clearly extended beyond 8 arcmin in our data. We have decided to use 10 arcmin as the limiting radius, which is the same limit used by Hanes & Harris (1986) in their photographic study. Integrating the powerlaw profile between  $\log r = -0.2$  ( $38''$ ) and 1 (10 arcmin), and adding the number of GCs interior to  $38''$  gives a total of 5700 GCs. The uncertainty in deriving the total number of GCs is dominated by the choice of limiting radius. We have used  $\pm 1$  arcminute about the limiting radius as our error estimate. Thus limiting radii of 9 and 11 arcminutes

give  $N = 5700 \pm 500$ . This is in good agreement with the determination of Kissler–Patig *et al.* (1997a) of  $N = 5940 \pm 570$ . For an absolute magnitude of  $M_V = -21.74$ , the specific frequency  $S_N = 11.5 \pm 1.0$ .

For NGC 1404 the limiting radius is difficult to estimate. Richtler *et al.* (1992) determined a background level at  $\sim 200''$ . We find that in the direction of NGC 1399, the density of GCs is clearly dominated by NGC 1399 beyond about  $250''$ . We have chosen to integrate out to  $240''$  (4 arcmin) with a reasonable range of 3–5 arcminutes. Thus integrating the profile from  $\log r = -0.3$  ( $30''$ ) to  $0.6$  (4 arcmin) and adding the number of inner GCs gives  $N = 725 \pm 145$  GCs associated with NGC 1404. This lies between the Hanes & Harris (1986) value ( $190 \pm 80$ ) and that of Richtler *et al.* (1992), i.e.  $880 \pm 120$ . Compared to these ground-based studies, our HST data has the advantages of accurate background subtraction (star, galaxies and NGC 1399 GCs) and nearly 100% complete magnitude coverage. For an absolute magnitude of  $M_V = -21.37$ , our results indicate a relatively low specific frequency for NGC 1404 of  $S_N = 2.0 \pm 0.5$ . Again using the HST data, we calculate the ‘local’  $S_N$  values (i.e. using the number of GCs and the integrated magnitude at the de Vaucouleurs effective radius) to be  $\sim 1.5$  for NGC 1399 and  $\sim 0.5$  for NGC 1404.

In Figures 4 and 5 we show the azimuthal distribution of GCs, as determined from the HST data, over the range for which we have uniform radial and azimuthal coverage. For NGC 1399 (Fig. 4) slight enhancements in the GC counts can be seen close to the galaxy major axes (position angles  $\sim 100^\circ$  and  $-80^\circ$ ). There is also a slight deficit around the minor axis P.A.  $\sim 10^\circ$ . Thus the GC system is broadly aligned with the stellar isophotes. The direction towards NGC 1404 (P.A.  $\sim 150^\circ$ ) is not covered by our HST image. For NGC 1404, shown in Fig. 5, there is slight deficit in GC counts along the galaxy major axis lies at P.A.  $\sim -20^\circ$ . There are also two enhancements at position angles  $\sim -50^\circ$  and  $10^\circ$  which do not correspond to either galaxy major or minor axes.

### 3.2 Colour and Metallicity Distributions

The GC colour distributions, after colour and magnitude selection, for the four HST pointings are shown in Fig. 6. Both NGC 1399 and NGC 1404 are dominated by red ( $B-I \sim 2.1$ ) GCs but with a significant tail to the blue (e.g.  $B-I \sim 1.6$ ). The GCs in the outer pointing of NGC 1399 are bluer on average than those in the central pointing. The median colours are  $B-I = 1.97$  for NGC 1399 in the central pointing,  $1.70$  for the outer NGC 1399 pointing and  $1.96$  for NGC 1404.

The CTIO data, after colour and magnitude selection, are shown in Fig. 7. We do not have a background field for the CTIO data. Although we have attempted to remove galaxies using the DAOPHOT sharpness and roundness parameters, our seeing conditions of  $\sim 1.5''$  imply that some galaxies will be included in our candidate list. The issue of background galaxy contamination in GC colour/metallicity distributions is discussed in some detail by Elson *et al.* (1997). Background galaxies in our magnitude range peak at  $B-I \sim 1.0$  and get bluer at fainter magnitudes. The galaxy counts are falling fast at our blue cutoff of  $B-I = 1.2$ . Given

the richness of the NGC 1399 GC system, background galaxies are likely to be a small affect. However it may be more of a concern for NGC 1404. We can estimate the effects of background contamination using the CFRS sample (Lilly *et al.* 1995) within the appropriate B magnitude range and scaled in area to match that of the CTIO data. The background-corrected distributions are shown by a dashed line in Fig. 7. As we have already removed some galaxies in our initial detection process, the true distribution may lie somewhere between the two histograms. In either case (uncorrected or corrected) the distributions reveal a somewhat different situation to the HST data, with both galaxy’s GC systems peaking in the blue ( $B-I \sim 1.6$ ) with a significant red tail (around  $B-I \sim 2.1$ ). The median colours are  $B-I = 1.84$  for NGC 1399 and  $1.71$  for NGC 1404. Thus the CTIO colours are on average systematically  $\sim 0.1$  mag bluer than the HST data. This result is not formally significant as the error is also on the order of  $0.1$  mag, but differences between the shape of the two distributions are clearly seen. As the HST data cover only the central regions of each galaxy, this suggests a radial colour gradient from red dominated objects at small galactocentric radii to blue ones further out. In principle, such a gradient could be caused by blue background galaxies in the CTIO data. However we give further evidence below that this is not the case.

In Fig. 8 we show the GC colour distributions for NGC 1399 and NGC 1404 from the HST data. Here the data for NGC 1399 includes both the central and outer pointing. The background-corrected histograms are shown by dashed lines. Some galaxies, such as M87 (Whitmore *et al.* 1995; Elson & Santiago 1996) reveal a clear bimodal GC colour distribution. In other cases (i.e. NGC 1374, 1379, 1387, 1427) the distribution is essentially consistent with a single unimodal colour for the GC system (Kissler–Patig *et al.* 1997a,b). The situation for NGC 1399 and NGC 1404 is not as clear. Nevertheless there is some evidence for multiple GC populations. Firstly, both galaxies have distributions that are significantly broader than that expected from the photometric errors (typically  $\sigma \sim 0.15$ ), i.e. there is a real spread in GC colours. Secondly, we have tested the unbinned colour data using the KMM statistical test (Ashman, Bird & Zepf 1994). This test rejects a single Gaussian fit to the NGC 1399 and NGC 1404 data with a confidence of over 99%. If we represent the data with two Gaussians then KMM determines means of  $B-I = 1.7$  and  $2.1$  for NGC 1399, and  $B-I = 1.6$  and  $2.1$  for NGC 1404. Thirdly, as an exercise, we generated a colour histogram that is the sum of two Gaussians. These Gaussians have mean colours of  $B-I = 1.6$  and  $2.1$  with dispersions similar to the photometric error, and with total numbers in the ratio of 1:4. They are shown in the lower left panel of Fig. 8. In the lower right panel, we show the same two Gaussians but with alternating Poisson noise included. To the eye, the two noisy Gaussians are qualitatively similar to the HST data, suggesting they could consist of two Gaussian-like populations. Fourth, the two peaks indicated in the HST data are also present in the CTIO data (Fig. 7). *We conclude that both galaxies do not have a single, uniform GC population but rather show evidence for a multimodal GC colour distribution.*

Two other large data sets exist for GCs in NGC 1399. They are the CTIO 4m observations by Ostrov *et al.* (1993) using Washington photometry and the Las Campanas 2.5m

observations by Kissler-Patig *et al.* (1997a) in V and I. In order to compare all of the different data sets we have converted each into metallicity. Broad-band colours can be transformed into metallicity using the Galactic relation of Couture *et al.* (1990) given the usual caveat that age effects and abundance anomalies may be present. The Washington photometry of Ostrov *et al.* is transformed using the relation derived by Geisler & Forte (1990). Washington photometry is the most sensitive to metallicity (rms  $\sim 0.1$ ), then B-I colours (rms  $\sim 0.15$ ) with V-I colours being the least sensitive (rms  $\sim 0.25$ ). In Fig. 9 we show the GC metallicity distributions from our HST and CTIO data sets, along with those of Ostrov *et al.* and Kissler-Patig *et al.* None of the data sets have been background corrected in this figure (although for the HST sample the correction is negligible). In general, the samples reveal a broad distribution with several minor enhancements, many of which appear common to several data sets. From their data, Ostrov *et al.* claimed that NGC 1399 has a trimodal GC metallicity distribution, with peaks at  $[\text{Fe}/\text{H}] \sim -1.5, -0.8, -0.2$ . The metal-rich peak corresponds to that seen clearly in our HST data. The two metal-poor peaks may be real or simply a single population with  $[\text{Fe}/\text{H}] \sim -1.0$ . The mean B-I colours found by the KMM test on the HST data correspond to  $[\text{Fe}/\text{H}] \sim -1.1$  and  $-0.1$ . The GC metallicity distribution for NGC 1404 from our HST data is shown in Fig. 10. As indicated by the KMM test, a bimodal distribution is a better representation of the data than a single Gaussian. The two GC populations have means of  $[\text{Fe}/\text{H}] \sim -1.5$  and  $-0.1$ .

We now return to the CTIO data and the issue of background contamination. Earlier we argued that contamination, although present, did not change the basic appearance of the colour distributions. Further evidence that the two peaks in the CTIO data are dominated by *bona fide* GCs comes from examining the spatial distribution of the two subpopulations. First, we define the metal-rich and metal-poor GC subpopulations in each galaxy as being  $\pm 0.3$  dex about the mean metallicity of each subpopulation. We then calculate the raw surface density (i.e. not corrected for background contamination or for the missing faint end of the luminosity function) for the two subpopulations. These surface density profiles are shown in Fig. 11. A background correction would tend to lower the metal-poor profile, particularly at galactocentric radii beyond 4 arcmin in NGC 1404 (which is excluded from the figure). Although there is considerable scatter, the surface density of each subpopulation declines with distance from its parent galaxy. This indicates that each subpopulation is associated with the galaxy and is therefore dominated by GCs. Secondly, the fact that the HST colours (metallicities) agree with those in the inner annuli of the CTIO data (see figures 12 and 13) indicates that the subpopulations are dominated by GCs.

Next we investigate the radial variation of GC metallicity. We have seen that for both NGC 1399 and NGC 1404, the metal-rich (red) subpopulation dominates in the HST data and in the CTIO data the metal-poor (blue) subpopulation is dominant. As the HST data probe the inner  $\sim 100''$  region and the CTIO data cover the regions beyond  $\sim 30''$  this would suggest that the metal-rich GCs are more centrally concentrated than the metal-poor ones. A similar situation is inferred for NGC 4472 (Geisler *et al.* 1996) and NGC 5846 (Forbes, Brodie & Huchra 1997). An un-

weighted fit to the HST data indeed indicates a metallicity gradient in both galaxies. For NGC 1399 we find  $[\text{Fe}/\text{H}] = -0.31 \pm 0.13 \log R$  (arcsec)  $- 0.046 \pm 0.22$ . This slope is similar to that found by Ostrov *et al.* (1993) i.e.  $-0.34 \pm 0.18$ . The fit for NGC 1404 gives  $[\text{Fe}/\text{H}] = -0.36 \pm 0.13 \log R$  (arcsec)  $- 0.034 \pm 0.22$ . In both cases the HST fits are consistent with the CTIO data. In NGC 4472, Geisler *et al.* (1996) found that the radial GC metallicity gradient was actually due to the changing relative mix of the two GC subpopulations. Assuming that NGC 1399 and NGC 1404 can be represented by metal-rich and metal-poor GC subpopulations we investigate the radial gradients further.

In Figures 12 and 13 we show the metallicity in various radial bins for the different GC subpopulations and the mean metallicity for the combined population. The range in metallicity included in each data point is  $\pm 0.3$  dex. For NGC 1399 (Fig. 12) the metal-poor and metal-rich GC subpopulations show no obvious radial metallicity gradient. However the mean values for the whole GC system *do* show a global radial gradient. Although not quite as convincing, the same trend appears to be true for NGC 1404 (Fig. 13). For both galaxies, we conclude that the radial metallicity gradient for the overall GC system is consistent with the changing relative proportions of the GC subpopulations; the metal-rich GCs are centrally concentrated while the metal-poor ones are preferentially located in the outer regions. The lack of a real abundance gradient places constraints on the role of gas dissipation in the formation of GCs. In NGC 4472, the metallicity of the galaxy field stars was found to be of the same or of slightly higher metallicity than the metal-rich GCs (Geisler *et al.* 1996). For NGC 1399, Brodie & Huchra (1991) quote a spectroscopic metallicity of  $[\text{Fe}/\text{H}] = +0.2 \pm 0.9$ . This is similar to the metallicity derived from B-I colours of the galaxy (from our CTIO data and from Goudfrooij *et al.* 1994). For NGC 1404, the galaxy B-I colours indicate  $[\text{Fe}/\text{H}] \sim -0.2$ . Thus for both galaxies, the field stars appear to have similar metallicities to those of metal-rich GCs (which have  $[\text{Fe}/\text{H}] \sim -0.1$ ).

### 3.3 Comparison with Globular Cluster Formation Scenarios

#### 3.3.1 The Merger Model

The merger model of Ashman & Zepf (1992) and Zepf & Ashman (1993) make some specific predictions concerning the properties of GCs in ellipticals that are the result of a gaseous merger. One of their key predictions is that ellipticals will have multimodal GC metallicity distributions. Furthermore the metal-rich GCs will be centrally concentrated and the more metal-poor ones will be preferentially located at large galactocentric radii. This indeed appears to be the case for both NGC 1399 and NGC 1404, and is therefore in qualitative agreement with their model. For NGC 1404 with a low  $S_N$  value (i.e.  $2.0 \pm 0.5$ ), Ashman & Zepf (1992) expect slightly fewer metal-rich (new) than metal-poor (old) GCs. Our data are generally consistent with this expectation. For NGC 1399 with  $S_N = 11.5 \pm 1.0$ , they would expect  $N_R/N_P \sim 3-4$ . In the central regions of NGC 1399 such a ratio may hold, but globally  $N_R/N_P < 1$ . This is of course complicated by the difficulty in defining clear metal-rich and metal-poor GC subpopulations. However there seems to be a shortfall

in the number of newly created GCs if gaseous mergers are responsible for the metal-rich GCs and the high  $S_N$  value. Another expectation from their merger model is that the galaxy starlight and GC system should have a similar spatial distribution in galaxies with high  $S_N$  values (i.e. those galaxies in which large numbers of new GCs should have been created by the merger). Thus we might expect the surface density of GCs to match that of the galaxy surface brightness profile for NGC 1399 but not for NGC 1404. Our data indicate that for both galaxies the GC distribution is notably flatter than the underlying starlight. We might also expect the metal-rich GCs, which should have formed from the gas of the progenitor galaxies, to reveal a radial metallicity gradient as the formation process should be dissipative. Figures 12 and 13 suggest that there is little or no metallicity gradient for the metal-rich GCs in either galaxy.

To summarize, the GC systems in NGC 1399 and NGC 1404 reveal some properties that are consistent with the Ashman & Zepf (1992) merger model, but there are also notable conflicts. On an individual basis, some of the disagreements with the model may be accommodated by slight modifications to the initial model (see Zepf, Ashman & Geisler 1995). Forbes, Brodie & Grillmair (1997) have recently investigated whether a sample of elliptical galaxies meets the general predictions of the Ashman & Zepf (1992) model, and concluded that mergers were *unlikely* to account for the GC systems in large elliptical galaxies. They favored a multiphase collapse scenario. Next we compare the data for NGC 1399 and NGC 1404 with this scenario.

### 3.3.2 The Multiphase Collapse Model

Forbes, Brodie & Grillmair (1997) have proposed that GCs in ellipticals form *in situ* during a multiphase collapse. In the first pre-galactic phase, metal-poor GCs are formed and later on, in the second galactic phase, the metal-rich GCs form. This leads to a bimodal metallicity distribution with the metal-rich GCs more centrally concentrated than the metal-poor ones. In massive ellipticals the collapse could be largely dissipationless and so no strong radial abundance gradients are expected. The radial distribution of (the metal-poor) GCs will be more extended than the galaxy itself, if as expected, they form before the galactic stars. The overall metallicity and spatial properties of GCs derived from our data are consistent with this picture.

For cD galaxies, such as NGC 1399, Forbes, Brodie & Grillmair (1997) suggested an additional source of GCs from tidal stripping of nearby galaxies. They suggested that some of GC subpopulation identified by Ostrov *et al.* (1993) at around  $[\text{Fe}/\text{H}] \sim -0.8$  were acquired from NGC 1404 and possibly other Fornax galaxies. Recently, Jone *et al.* (1997) have interpreted the asymmetric X-ray emission around NGC 1404 as evidence for tidal interaction with NGC 1399. The idea of tidal stripping of GCs is given some support by our new data. The outer regions of NGC 1404 are dominated by metal-poor GCs, and it is these GCs that may be preferentially stripped and captured by NGC 1399. Thus some of the GCs in NGC 1399 with this intermediate metallicity may have originated from NGC 1404. We confirmed that NGC 1404 has a remarkably low specific frequency value ( $S_N = 2.0 \pm 0.5$ ) for a cluster elliptical, suggesting that some GCs may have been lost. If NGC 1404 originally had  $S_N = 5$ , i.e. typ-

ical of normal ellipticals outside of the Fornax cluster then it has lost  $\sim 1000$  GCs, which may have been tidally captured by NGC 1399. If we assume that the GC system and galaxy starlight originally (i.e. before tidal stripping) continued beyond 4 arcminutes with the same slope as found in section 3.1, then we can calculate the  $S_N$  value of the stripped GCs. We find that the stripped GCs are unlikely reach values of  $S_N \sim 11.5$  in sufficient numbers to have any appreciable effect on the specific frequency of NGC 1399. We expected the GC surface density profile to match that of the underlying starlight in the inner regions of NGC 1404, but it appears to be somewhat flatter than the stellar profile (at least for galactocentric radii of less than  $\sim 150''$ ). This may just be indicating that tidal stripping has not yet affected the galaxy inner regions. The above circumstantial evidence suggests that NGC 1399 has acquired GCs from NGC 1404, although this is unlikely to explain the high specific frequency of NGC 1399. Large samples of GC metallicity and kinematic information from spectra are probably required before the multiphase collapse and tidal stripping ideas can be fully tested.

## 4 CONCLUSIONS

We present new optical data of the globular cluster (GC) systems in NGC 1399 and NGC 1404. Our images were taken in B and I filters using the Hubble Space Telescope (HST) and the 1.5m telescope at Cerro Tololo Inter-American Observatory (CTIO). This provides us with high spatial resolution in the central regions and wide area coverage respectively. From the HST data we have detected over 500 GCs in NGC 1399 and over 200 in NGC 1404, covering  $\sim 90\%$  of the GC luminosity function. With the aid of an HST background field of the same exposure time, we estimate that the contamination levels in the HST samples are only a few percent.

Both galaxies reveal a broad GC colour/metallicity distribution. These distributions are *inconsistent* with a single Gaussian. For NGC 1399, two Gaussians with mean metallicities of  $[\text{Fe}/\text{H}] \sim -1.1$  and  $-0.1$  provide a reasonable representation of the data, although a multimodal distribution with several different GC subpopulations remains a possibility. In the case of NGC 1404 we tentatively claim evidence for a bimodal GC distribution with the metal-poor population around  $[\text{Fe}/\text{H}] \sim -1.5$  and the metal-rich population at  $[\text{Fe}/\text{H}] \sim -0.1$ . In both galaxies the different metallicity peaks are consistent with distinct GC subpopulations in which the metal-rich GCs are more centrally concentrated than the metal-poor ones. Globally, the GC systems reveal metallicity gradients. However these gradients are consistent with a changing relative mix of the two GC subpopulations with galactocentric radius.

We derive GC surface density profiles, and show them to be flatter (i.e. more extended) than the underlying starlight. The total number of GCs and specific frequency are calculated to be  $N = 5700 \pm 500$ ,  $S_N = 11.5 \pm 1.0$  for NGC 1399 and  $N = 725 \pm 145$ ,  $S_N = 2.0 \pm 0.5$  for NGC 1404. Finally we discuss our results in the context of two GC formation scenarios. The GC data on NGC 1399 and NGC 1404 are generally more consistent with a multiphase collapse (e.g.

Forbes, Brodie & Grillmair 1997) than a merger (e.g. Ashman & Zepf 1992) origin.

#### Acknowledgments

We thank M. Kissler-Patig and M. Rabban for help and useful discussions. We also thank the referee, T. Bridges, for several helpful comments. This research was funded by the HST grant GO-05990.01-94A.

#### References

- Ashman, K. M., Bird, C. M., Zepf, S. E., 1994, *AJ*, 108, 2348  
 Ashman, K. M., Zepf, S. E., 1992, *ApJ*, 384, 50  
 Brodie, J. P., Huchra, J., 1991, *ApJ*, 379, 157  
 Bridges, T. J., Hanes, D. A., Harris, W. E., 1991, *AJ*, 101, 469  
 Couture, J., Harris, W. E., Allwright, J. W. B., 1990, *ApJS*, 73, 671  
 de Vaucouleurs, A., Longo, G., 1988, *Catalogue of visual and infrared photometry of galaxies from 0.5 $\mu$ m to 10 $\mu$ m*. University of Texas, Austin  
 Elson, R. A. W., Santiago, B. X., 1996, *MNRAS*, 280, 971  
 Elson, R. A. W., Grillmair, C. J., Forbes, D. A., Rabban, M., Williger, G. M., Brodie, J. P., 1997, *MNRAS*, submitted  
 Faber, S. M., *et al.* 1989, *ApJS*, 69, 763  
 Forbes, D. A., Brodie, J. P., Huchra, J., 1996, *AJ*, 112, 2448  
 Forbes, D. A., Brodie, J. P., Huchra, J., 1997, *AJ*, 113, 887  
 Forbes, D. A., Brodie, J. P., Grillmair, C. J., 1997, *AJ*, 113, 1652  
 Forbes, D. A., Franx, M., Illingworth, G. D., Carollo, C. M., 1996, *ApJ*, 467, 126  
 Forbes, D. A., Franx, M., Illingworth, G. D., 1995, *AJ*, 109, 1988  
 Forte, J. C., Martinez, R. E., Muzzio, J. C., 1982, *AJ*, 87, 1465  
 Geisler, D., Lee, M. G., Kim, E., 1996, *AJ*, 111, 1529  
 Geisler, D., Forte, J. C., 1990, *ApJ*, 350, L5  
 Goudfrooij, P., Hansen, L., Jorgensen, H. E., Norgaard Nielson, H. U. de Jong, T., van den Hoek, L. B., 1994, *A & AS*, 104, 179  
 Grillmair, C., *et al.* 1994a, *ApJ*, 422, L9  
 Grillmair, C., *et al.* 1994b, *AJ*, 108, 102  
 Grillmair, C., Pritchett, C., van den Bergh, S., 1986, *AJ* 91, 1328  
 Grillmair, C., Forbes, D. A., Brodie, J. P., Elson, R. A. W., 1997, *AJ*, submitted  
 Hanes, D. A., Harris, W. E., 1986, *ApJ*, 309, 564  
 Harris, W. E., van den Bergh, S., 1981, *AJ*, 86, 1627  
 Huchra, J., Brodie, J. P., Kent, S., 1991, *ApJ*, 370, 495  
 Ikebe, Y., *et al.* 1996, *Nature*, 379, 427  
 Jacoby, G. H., *et al.* 1992, *PASP*, 104, 599 (J92)  
 Jones, C., Stern, C., Forman, W., Breen, J., David, L., Tucker, W., & Franx, M. 1997, *ApJ*, 482, 143  
 Kissler-Patig, M., *et al.* 1997a, *A & A*, 319, 470  
 Kissler-Patig, M., Forbes, D. A., Minniti, D., 1997b, in preparation  
 Kohle, S., *et al.* 1995, *A & A*, 309, L37  
 Lilly, S. J., Le Fevre, O., Crampton, D., Hammer, F., Tresse, L., 1995, *ApJ*, 455, 50  
 Longo, G., de Vaucouleurs, A., 1983, *A General Catalogue of Photometric Magnitudes and Colours in the UBV system*. University of Texas, Austin  
 Madore, B., *et al.* 1997, in preparation  
 Mason, K. O., Rosen, S. R., 1985, *Sp. Sc. Rev.*, 40, 675  
 Ostrov, P., Geisler, D., Forte, J. C., 1993, *AJ*, 105, 1762  
 Richtler, T., Gerbel, E. K., Domgorgen, H., Hilker, M., Kissler, M., 1992, *A & A*, 264, 25  
 Wagner, S., Richtler, T., Hopp, U., 1991, *A & A*, 241, 399  
 West, M. J., Cote, P., Jones, C., Forman, W., Marzke, R. O., 1995, *ApJ*, 453, L77  
 Whitmore, B. C., Sparks, W. B., Lucas, R. A., Macchetto,

F. D., Biretta, J. A., 1995, ApJ, 454, L73

Zepf, S. E., Ashman, K. M., 1993, MNRAS, 264, 611

Zepf, S. E., Ashman, K. M., Geisler, D., 1995, ApJ, 443, 570

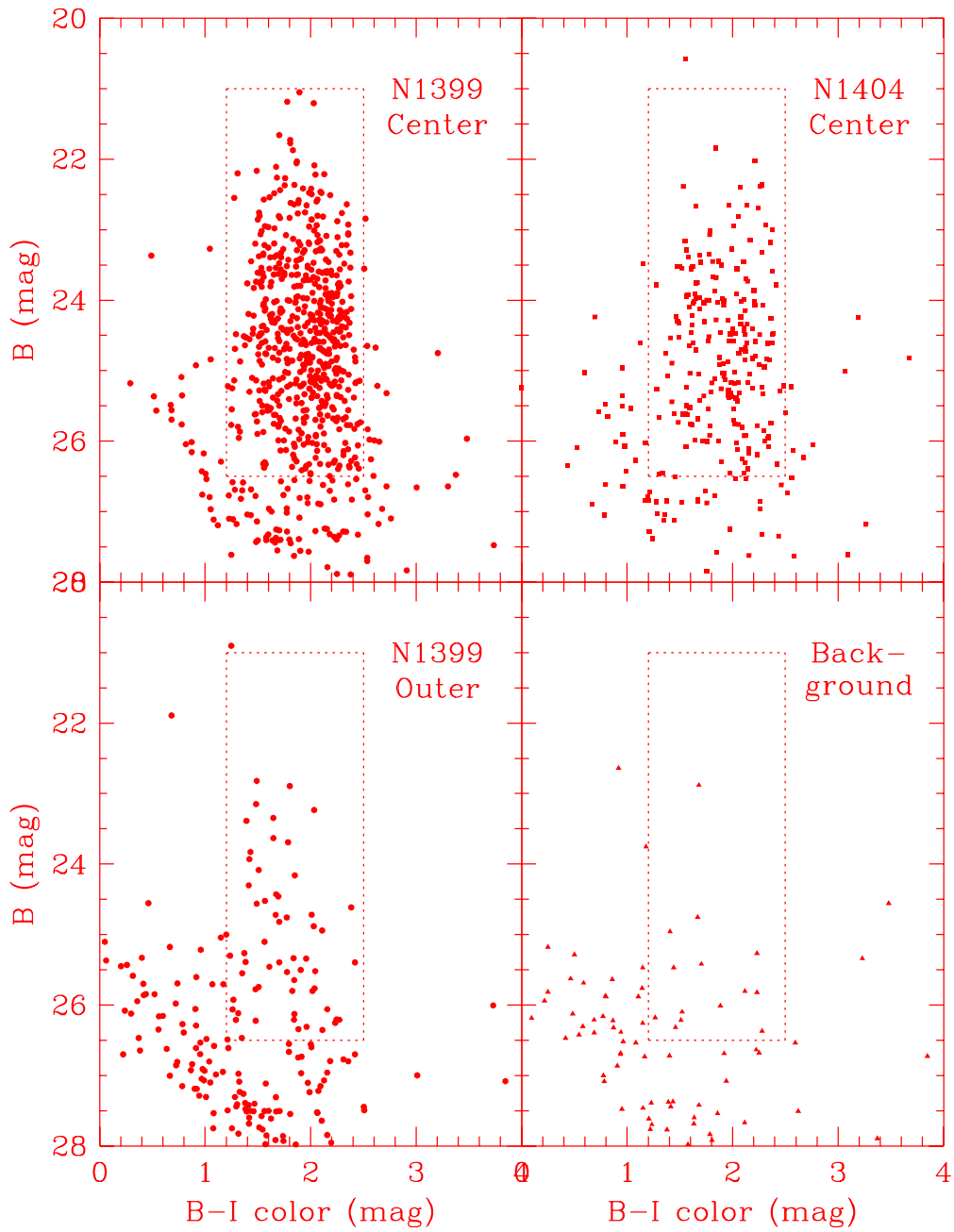


**Figure 1.** Colour–magnitude diagrams for the compact objects in four HST pointings: central NGC 1399 (circles), central NGC 1404 (squares), outer NGC 1399 (circles) and a background field (triangles). The dashed box indicates the colour and magnitude selection criteria (see text for details).

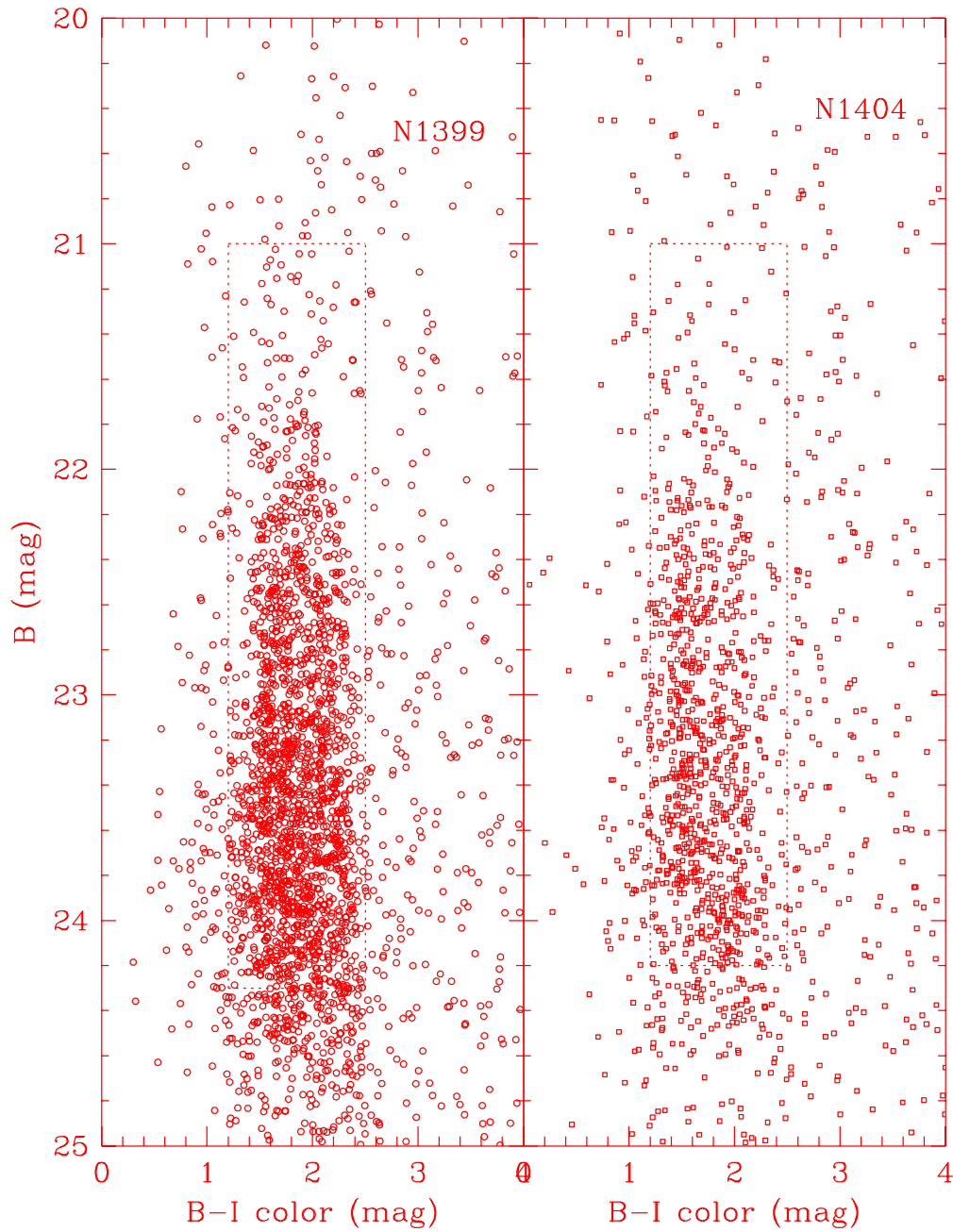


**Figure 2.** Colour–magnitude diagrams for the compact objects in two CTIO pointings centered on NGC 1399 (circles) and NGC 1404 (squares). The dashed box indicates the colour and magnitude selection criteria (see text for details).

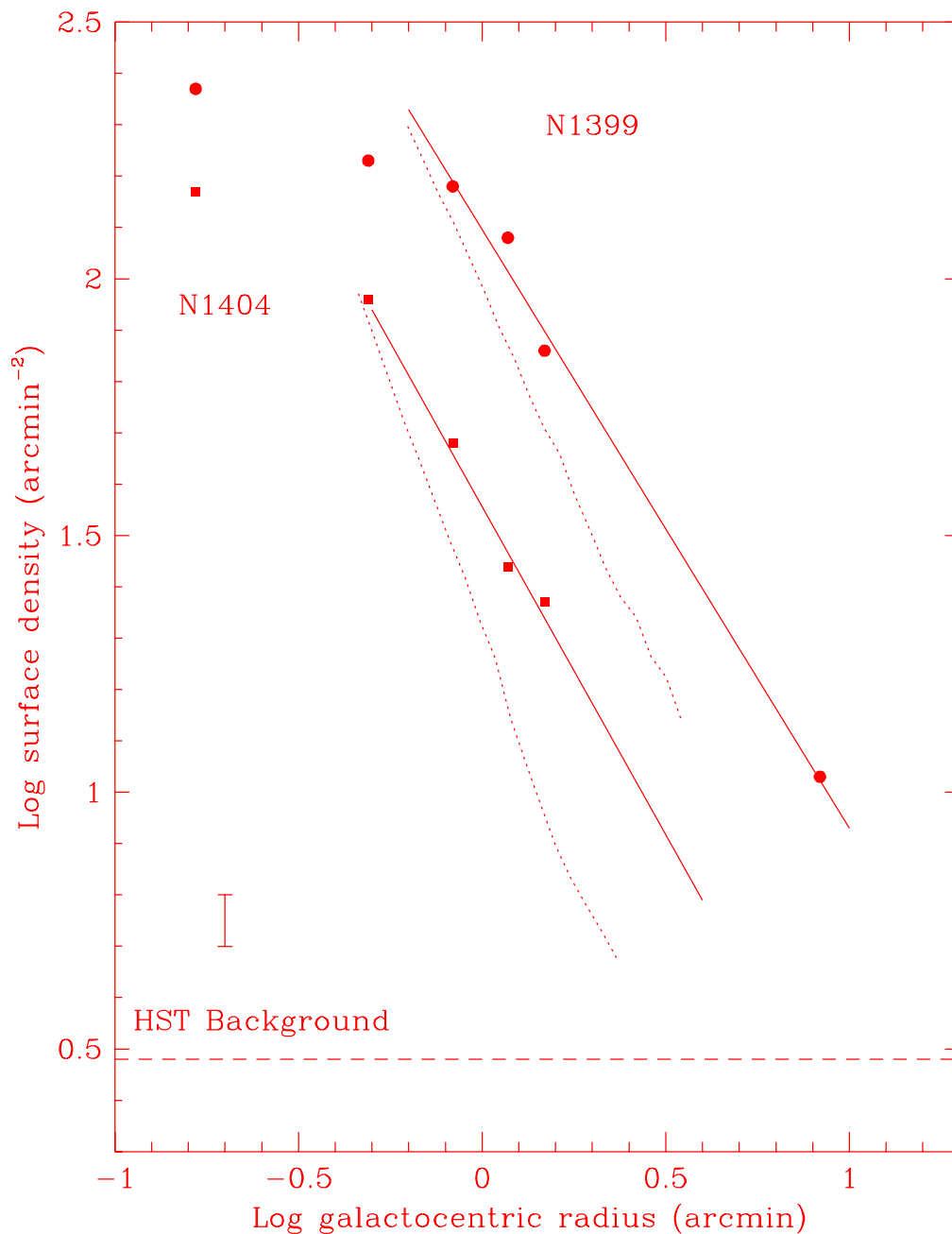


**Figure 3.** Surface density profiles for the globular cluster systems in NGC 1399 (circles) and NGC 1404 (squares) from HST data. The surface densities have had a correction for background contamination and for the missing faintest globular clusters. The globular cluster systems of both galaxies reveal a ‘core region’. Powerlaw fits to the data beyond the core region are shown by solid lines. The surface density of compact background objects in HST images is shown by a long-dashed line. A typical error bar is shown on the left. The underlying galaxy starlight profile, arbitrarily normalized in the vertical direction, is shown by a short-dashed line. For both galaxies the starlight is more concentrated than the globular cluster system.

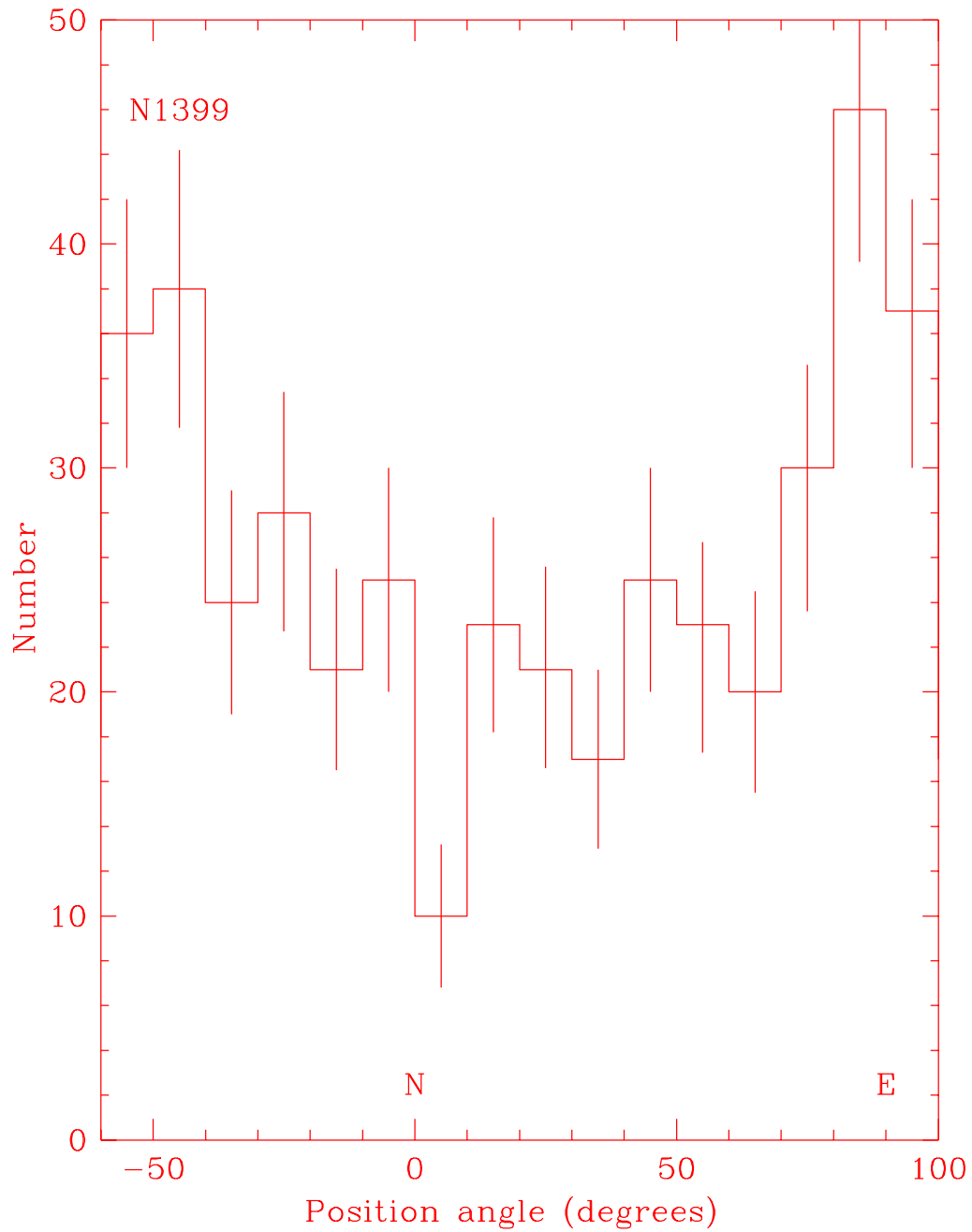


**Figure 4.** Histogram of globular cluster position angles within  $100''$  radius of NGC 1399, from HST data. The galaxy major axes are P.A.  $\sim 100^\circ$  and  $-80^\circ$ . Globular clusters appear to be concentrated close to the galaxy major axis and show a deficit along the minor axis.

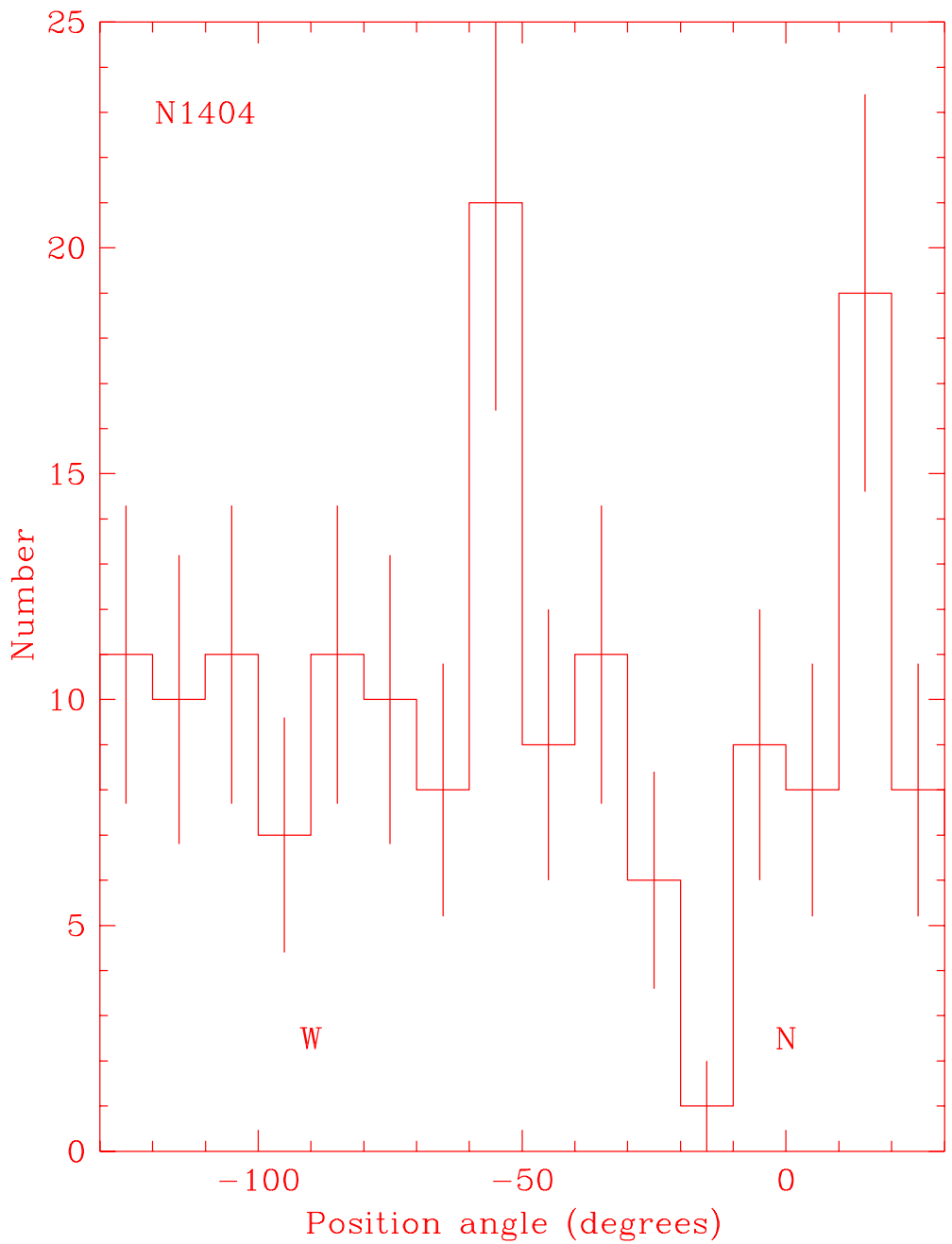


**Figure 5.** Histogram of globular cluster position angle within  $100''$  of NGC 1404, from HST data. The galaxy major axis is P.A.  $\sim -20^\circ$ . Globular clusters appear to show a slight deficit near the galaxy major axis.

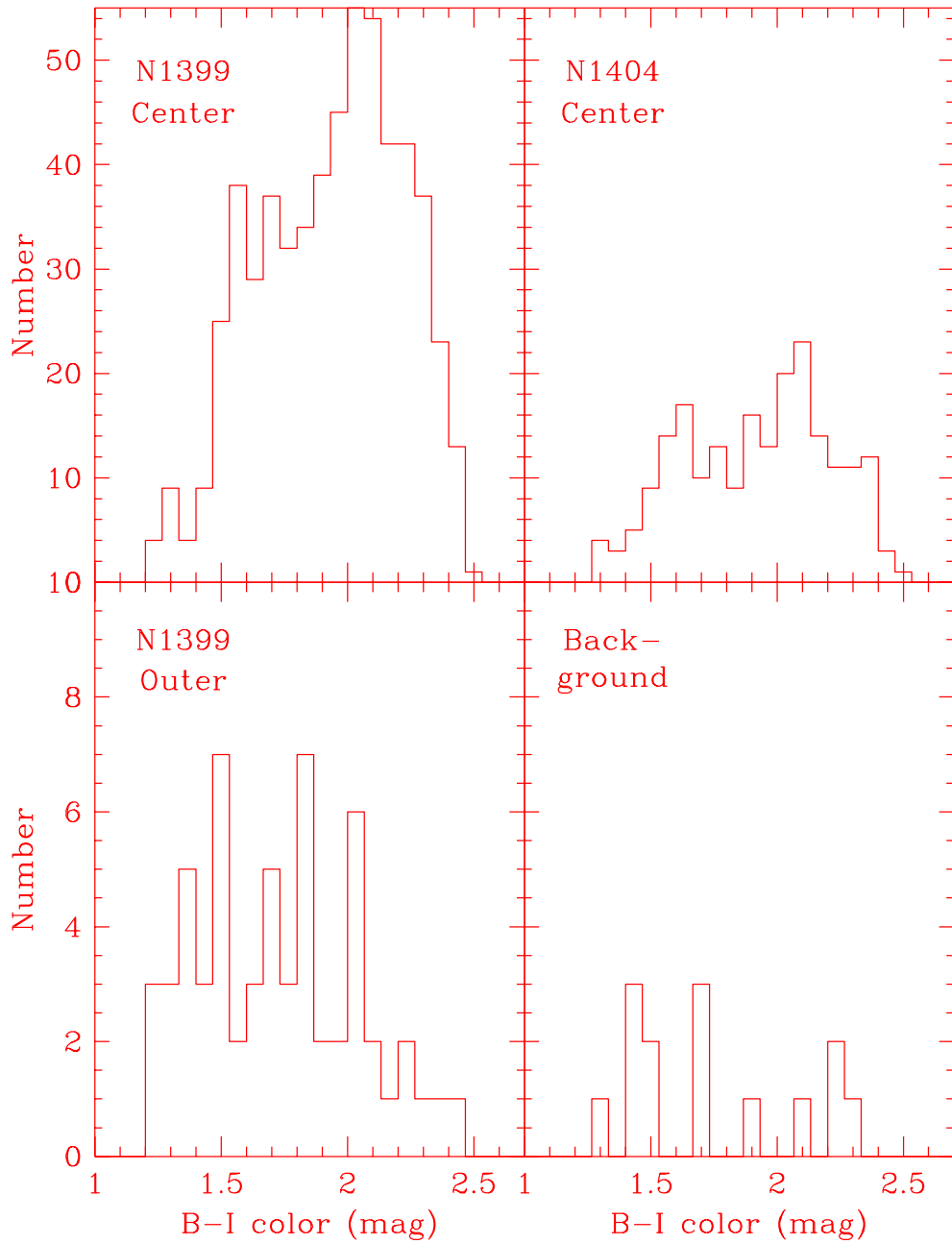


**Figure 6.** Histograms of globular cluster B-I colours for the four HST pointings. In the central pointings, both galaxies are dominated by red globular clusters with an extended blue tail.

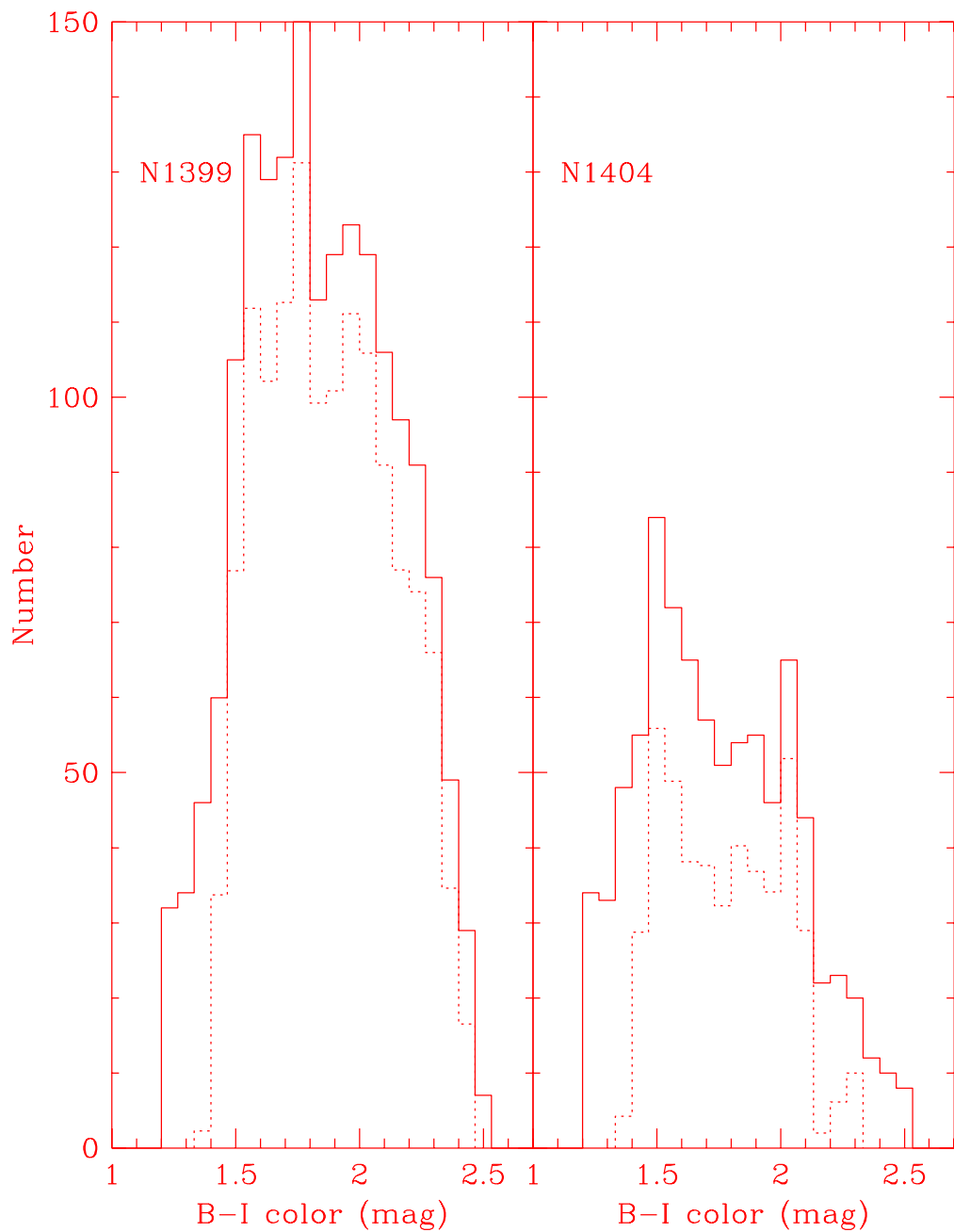


**Figure 7.** Histograms of globular cluster B-I colours for the two CTIO pointings. The dashed line shows the distribution after correction for background contamination. In these wide area pointings, both galaxies are dominated by blue globular clusters with an extended red tail.

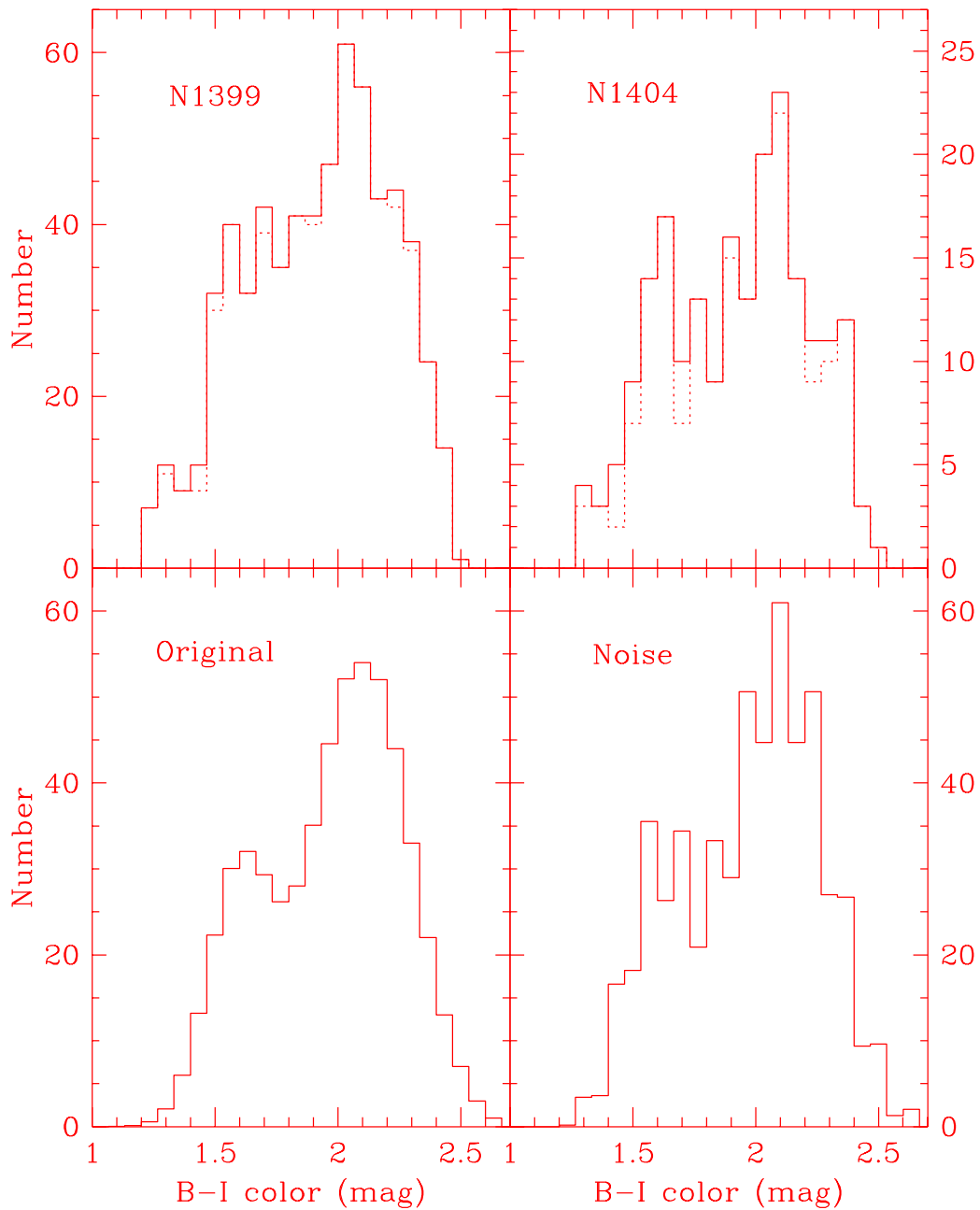


**Figure 8.** Histograms of the globular cluster B-I colours in NGC 1399 and NGC 1404 from HST data (upper panels). For NGC 1399 the central and outer pointings have been co-added. The dashed line shows the distribution after correction for background contamination. The lower left panel shows the sum of two Gaussians with peaks at B-I = 1.6 and 2.1. The lower right panel shows the same two Gaussians with Poisson noise included. The metallicity distribution of both galaxies can be plausibly represented by two Gaussians.

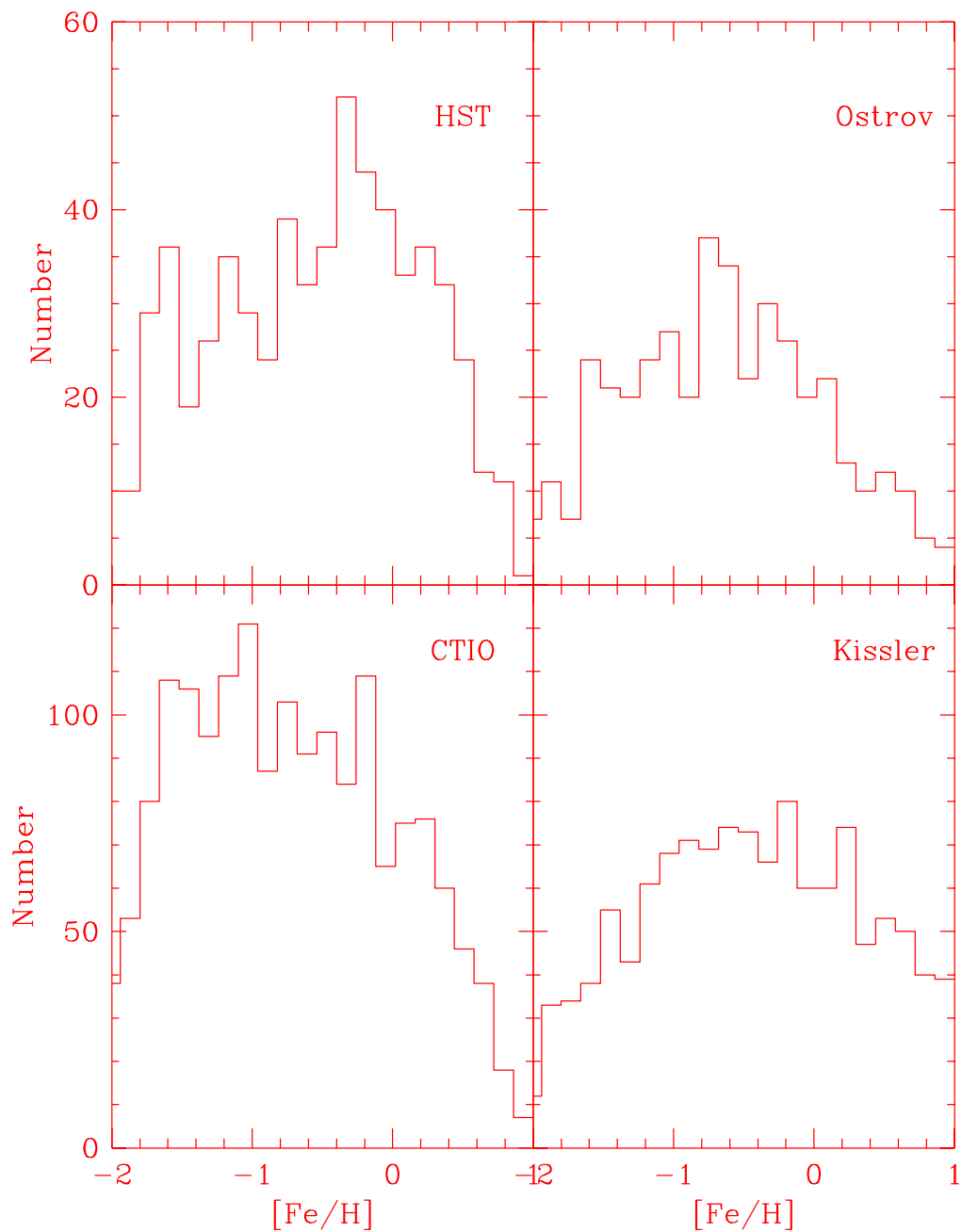


**Figure 9.** The metallicity distribution for globular clusters in NGC 1399 from four different samples. Data from this paper are shown in the left hand side panels. The upper right panel shows the data of Ostrov *et al.* (1993), and the lower right panel shows the data of Kissler-Patig *et al.* (1997a). None of the samples shown here have been background corrected (although for the HST sample this is negligible). The Ostrov *et al.* data have the highest metallicity sensitivity. The HST distribution is inconsistent with a single Gaussian and is better described as multimodal. Common peaks (particularly at  $[\text{Fe}/\text{H}] \sim -0.2$ ) can be seen in each data set.

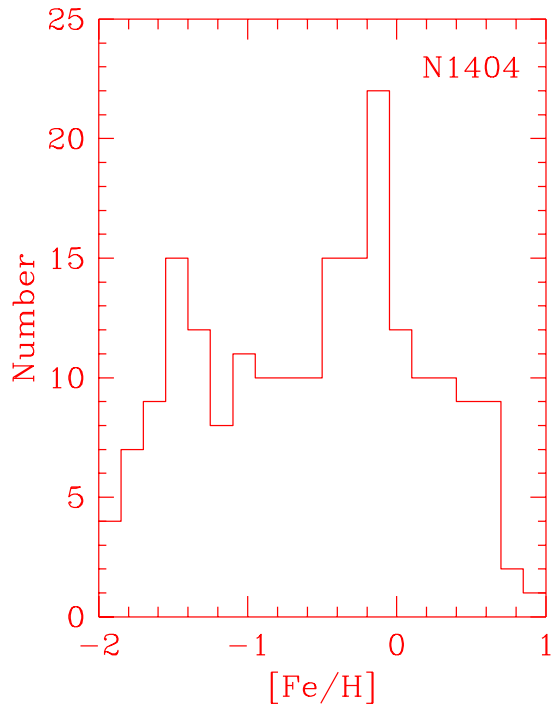


**Figure 10.** The metallicity distribution for globular clusters in NGC 1404 from HST data. A KMM test indicates that the distribution is inconsistent with a single Gaussian and that a bimodal distribution with mean metallicities of  $[\text{Fe}/\text{H}] \sim -1.5$  and  $-0.1$  provides a better fit.

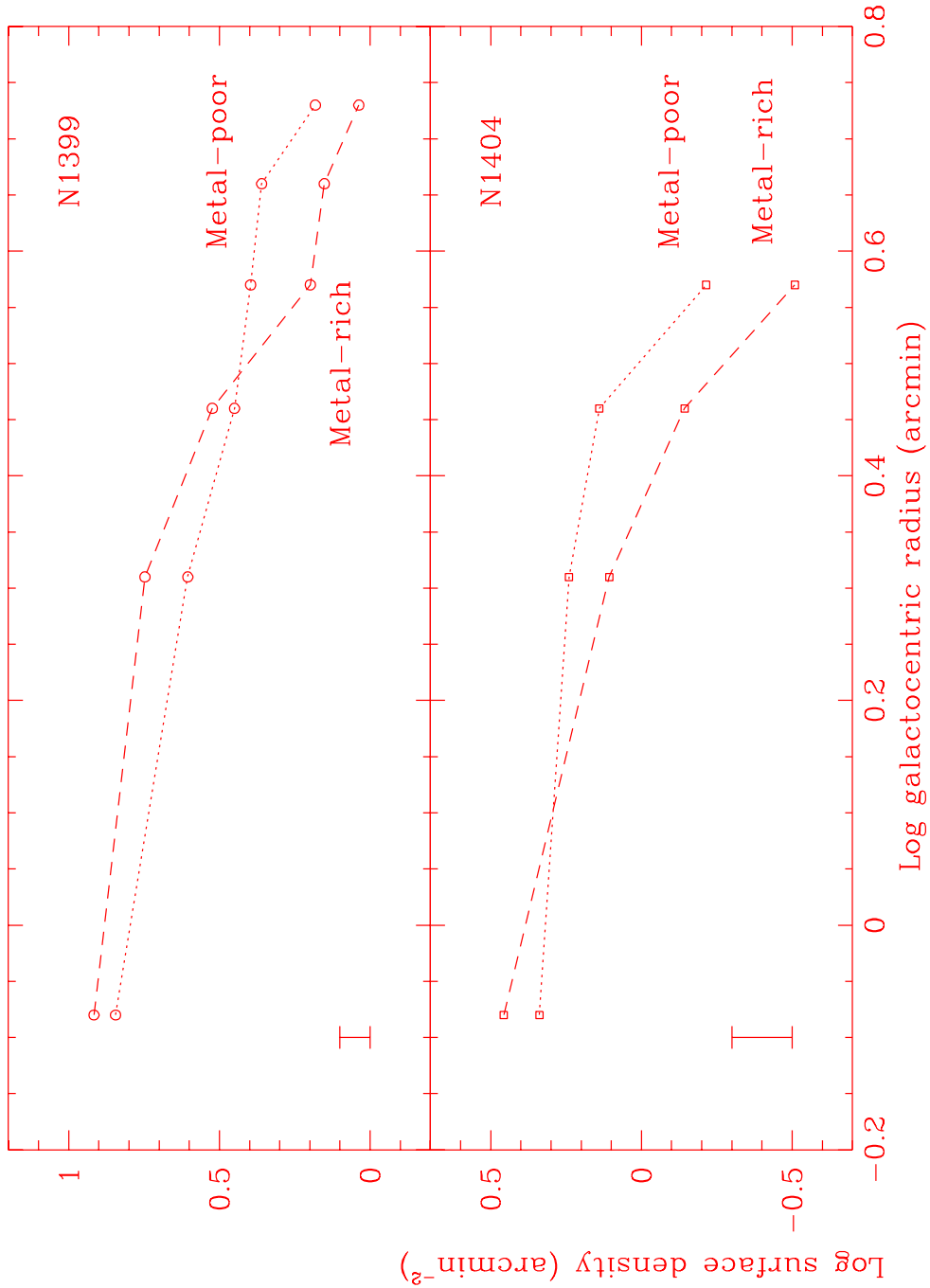


**Figure 11.** Surface density profiles for the metal-rich and metal-poor globular cluster subpopulations in NGC 1399 (circles) and NGC 1404 (squares) from CTIO data. No correction has been applied for background contamination or missing globular clusters at the faint end of the luminosity function. Typical data error bars are shown on the left. In both galaxies the two subpopulations decline with galactocentric radius indicating that they are dominated by globular clusters. The metal-rich subpopulation is more centrally concentrated.

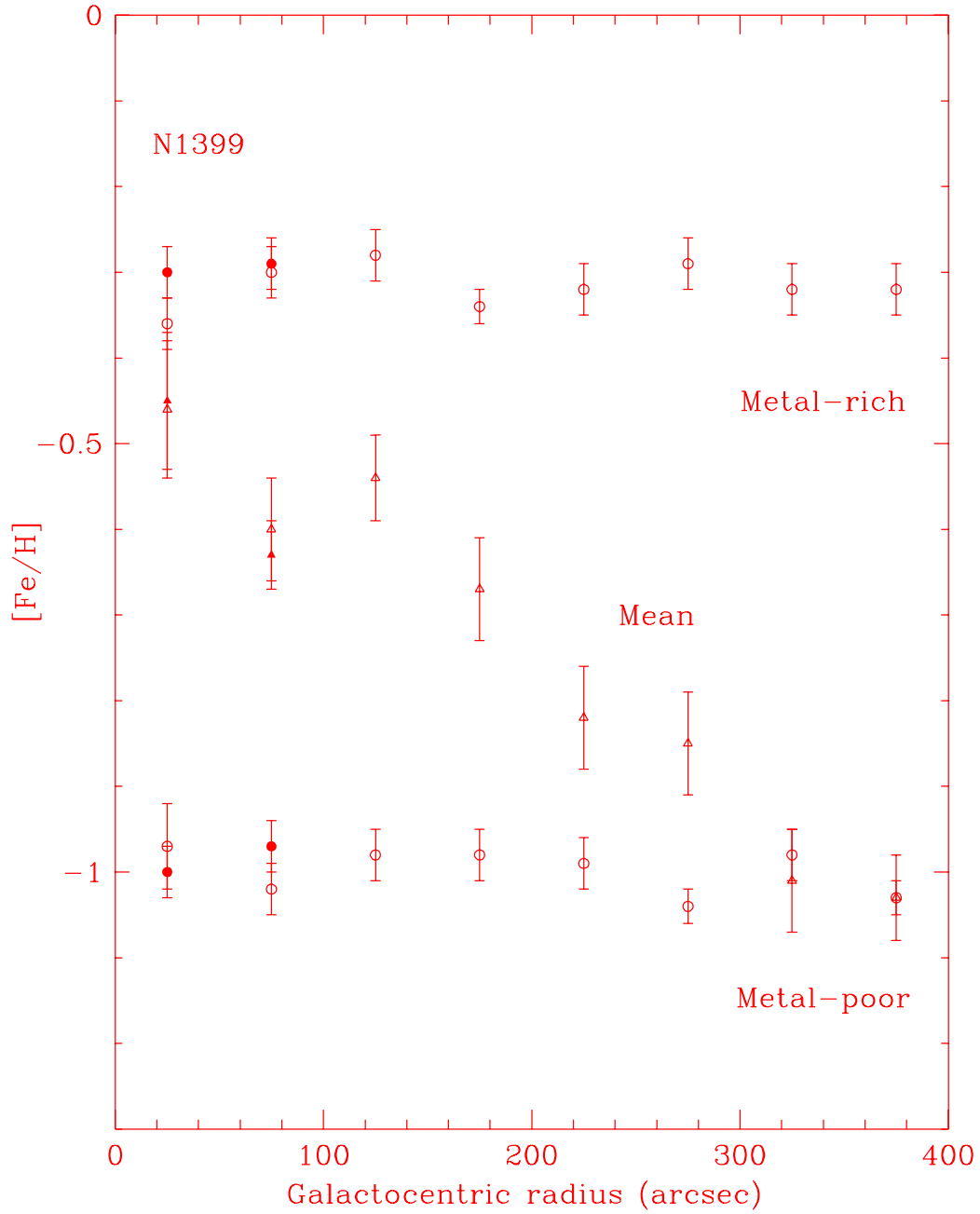


**Figure 12.** Radial variation of metallicity for the globular cluster subpopulations in NGC 1399. The filled circles show the HST data and the open circles the CTIO data. The metal-rich, metal-poor and mean for the whole globular cluster system are shown. The mean metallicity gradient is consistent with the changing relative proportions of the subpopulations with galactocentric radius.

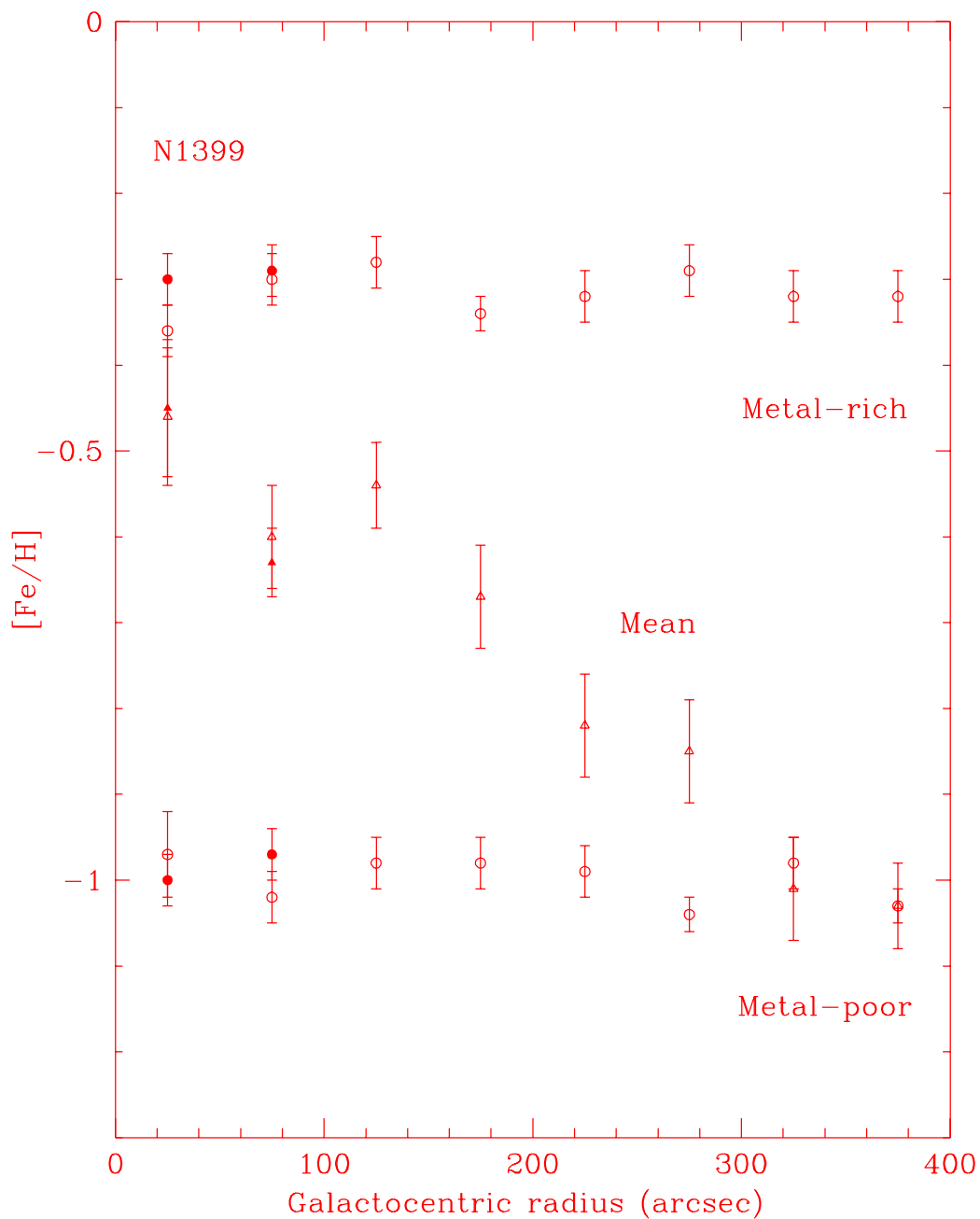


**Figure 13.** Radial variation of metallicity for the globular cluster subpopulations in NGC 1404. The filled circles show the HST data and the open circles the CTIO data. The metal-rich, intermediate, metal-poor and mean for the whole globular cluster system are shown. The mean metallicity gradient is consistent with the changing relative proportions of the subpopulations with galactocentric radius.